Desalination and Water Treatment
www.deswater.com

doi: 10.5004/dwt.2020.24923

177 (2020) 197–208
February

Adsorption of neutral red onto MIL-100(Fe) from solution: characterization, equilibrium, kinetics, thermodynamics and process design

Shanshan Chen, Kang Wen, Xiaoting Zhang, Ruize Zhang, Runping Han*

College of Chemistry, Zhengzhou University, No 100 of Kexue Road, Zhengzhou 450001, China,
Tel. +86 371 67781757; Fax +86 371 67781556; emails: rphan67@zzu.edu.cn (R. Han), 2503579590@qq.com (S. Chen), 1039171416@qq.com (K. Wen), 1619888517@qq.com (X. Zhang), 690724768@qq.com (R. Zhang)

Received 15 April 2019; Accepted 19 September 2019

ABSTRACT

Metal organic frameworks are attracting scientific interest in adsorption applications owing to their large surface area and controllable pore size or shape over both microporous and mesoporous domains. Based on this, an iron(III) trimesic acid MIL-100(Fe) was facilely synthesized by hydrothermal treatment and used as adsorbent to remove neutral red (NR) from aqueous solution. MIL-100(Fe) was characterized using X-ray diffraction, scanning electron microscopy and transform infrared spectroscopy. MIL-100(Fe) was studied in view of the adsorption isotherms, thermodynamics, kinetics, and regeneration of the adsorbent. The adsorption kinetics data of NR were found to be in agreement with pseudo-second-order model. Temkin model was observed to be more suitable than Freundlich and Langmuir models in describing the adsorption isotherm. The maximum adsorption quantity was 333 mg g^{-1} at 313 K from Langmuir model. Thermodynamic parameters indicated that the NR adsorption process was endothermic and spontaneous. The NR-loaded MIL-100(Fe) adsorbent was regenerated and reused using pH = 2, 75% ethanol. A single-stage batch design for NR adsorption onto MIL-100(Fe) was also presented based on Temkin isotherm model equation. Based on the findings, MIL-100(Fe) is a promising adsorbent for the removal of cationic dyes from solution and thus can be used in practical application.

Keywords: MIL-100(Fe); Neutral Red; Adsorption; Regeneration

1. Introduction

In recent times, China has been faced with the issue of water pollution as a result of the generation of considerable amount of wastewater with color has been generated from many industries [1]. Among them, printing and dyeing wastewater has become one of the most difficult points in China's wastewater treatment because of its high dye concentration, wide pH variation and various complex elements. Moreover, many dyes are considered to be toxic and even carcinogenic [2,3].

Neutral red (the structure seen from Fig. 1) is 3-amino-7-dimethylamino-2-methylphenazine hydrochloride with conjugated bond in the molecule, which is a eurhodin dye commonly used for staining lysosomes. NR can also be used as a pH indicator, changing from red to yellow between pH 6.8 and 8.0. There is a balance between neutral and protonated forms of NR. At acidic conditions, NR exists mainly in the form of protonation; at alkaline conditions, NR mainly exists in a neutral form.

* Corresponding author.

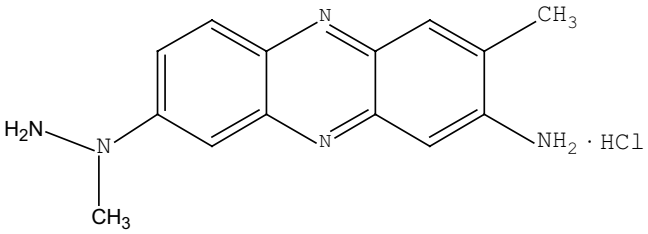

Fig. 1. Structure of NR.

It is difficult to degrade dye compounds because they are very stable to light and oxidation reactions. In this context, separation and removal of organic pollutants before discharging into water bodies and onto terrestrial lands are of great significance [4]. To date, significant research efforts have been devoted to developing economic and effective techniques for the removal of hazardous organic pollutants from wastewater and industrial effluents. These include adsorption [5–8], coagulation [9], electrocoagulation [10], biodegradation [11], photodegradation [12] and advanced oxidation process [13,14]. Among these methods, adsorption is considered as a fairly cost-effective and reliable technique for wastewater remediation due to its high efficiency, easy operation and availability of various kinds of adsorbents [15].

Compared with the conventional adsorbents, metal organic frameworks (MOFs) have gained attention as promising materials for aqueous-phase adsorptive removal of contaminants. Attributes such as large adsorption capacity, diverse hierarchical structure, high surface area, permanent porosity, tunable pore size, modifiable surface and recyclability give MOFs an edge over conventional adsorbents [16–18]. The performance of MOFs and their selectivity toward targeted pollutants of interest can be regulated by the judicious selection of metal ion and organic linker [19]. MOFs have been applied in several fields, such as catalysis [20], gas storage [21], separation [22], luminescence [23], chemical sensing [24], and magnetism [25]. Enamul et al. [26] reported an iron terephthalate (MOF-235) adsorbent to remove methyl orange (MO) and methylene blue (MB) from aqueous solution. Adsorption of MO and MB at various temperatures showed that the adsorption was a spontaneous and endothermic process [26]. Rajkumar et al [27] synthesised a series of MOFs for analysis of structures and applications in adsorption field, and found that MOFs exhibited many unique characteristics. Huo and Yan [28] synthesised MIL-100(Fe) for the removal of malachite green (MG) from solution. Compared with these adsorbents, the merits of MIL-100(Fe) as an adsorbent are its remarkable chemical and solvent stability, unsaturated metal sites, aromatic pore walls for strong interactions [28]. However, the study of adsorption behavior on MIL-100(Fe) is limited by far.

MIL-100(Fe) was prepared and chosen as the adsorbent in this work. Herein, the adsorption behavior of dye on MIL-100(Fe) from aqueous solution was presented. Cationic NR was chosen as the representative dye. To understand the adsorption property and its mechanism, the adsorption kinetics and thermodynamics studies of NR on MIL-100(Fe) were carried out in detail.

2. Materials and methods

2.1. Reagents and chemicals

All reagents were of analytical grade and used without further purification. Trimesic acid (H_3BTC) was supplied by Aladdin Industrial Corporation (Shanghai pudong new district, China), and iron(III) nitrate nonahydrate ($Fe(NO_3)_3{\cdot}9H_2O$) was purchased from Sinopharm Chemical Reagent Co. Ltd. (Ningbo road, Shanghai, China). Neutral Red ($C_{15}H_{17}N_4Cl$) was obtained from Shang Hai SSS Reagent Co. Ltd., (Military road, Shanghai, China). N,N-Dimethyl formamide (DMF) and ethanol (C_2H_5OH) were bought from Fuchen (Tianjin) Chemical Reagent Co, Ltd.

2.2. Preparation of MIL-100(Fe)

MIL-100(Fe) was synthesized by hydrothermal method following the previous literature procedure [29]. The process can be seen from Fig. 2: the mixed solution was placed in a Teflon-lined autoclave containing the reaction solution with a chemical composition of $Fe(NO_3)_3{\cdot}9H_2O$, H_3BTC and deionized water. The molar ratio of $Fe(NO_3)_3{\cdot}9H_2O$:H_3BTC:H_2O was fixed at 1:0.67:35. The crystallization was followed at 95°C for 12 h, and then cooled down to room temperature. The as-synthesized MIL-100(Fe) was further purified with heating water at 60°C for 5 h to remove residual unreacted ions after the solution was vacuumed drying. The yellow powder obtained after drying the solution was fully ground and then vacuum dried overnight. The final product was labeled as MIL-100(Fe) and was used for further studies and characterizations.

2.3. Characterization of MIL-100(Fe)

In this experiment, the surface structure as well as the physical and chemical properties of MIL-100(Fe) were determined, which provided theoretical basis for experimental results and adsorption mechanism. The pH at point zero charge (pH_{pzc}) of MIL-100(Fe) was determined by the 0.010 mol L^{-1} NaCl solution addition method. The morphology of MIL-100(Fe) was characterized by scanning electron microscope (SEM, FEI Quanta 200F, Holland). The characteristic functional groups were determined by Fourier transform infrared spectroscopy (FTIR Spectrometer, Nicolet iS50, USA). X-ray diffractometer (XRD, X'Pert PRO, Holland) was used to determine the structure of MIL-100(Fe) over the angular range from 2° to 40°. The MIL-100(Fe) specific surface area was evaluated based on the Brunauer–Emmett–Teller method (BET, ASAP2420-4MP, USA). The chemical composition of MIL-100(Fe) before and after adsorption of NR was analyzed by X-ray photoelectron spectroscopy (XPS, ESCALAB 250Xi, England).

2.3. Adsorption experiments

The batch adsorption experiments were carried out in air bath at 303 K and 120 rpm. A certain amount of absorbent (10 mg) was introduced in 50 mL Erlenmeyer flask with 20 mL NR. Effect of factors, such as contact time, adsorbent

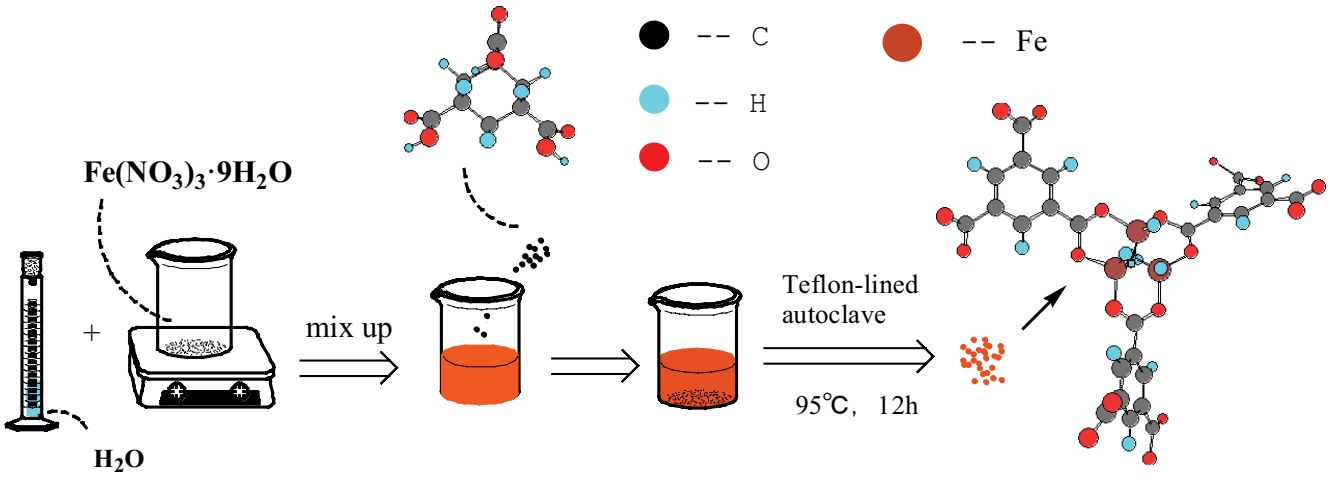

Fig. 2. Synthesis process of MIL-100(Fe).

dose, coexisting ions and initial solution pH on the adsorption process were performed with NR concentration of 50 mg L^{-1} at 303 K. Various initial NR concentrations of 10–170 mg L^{-1} were selected to obtain adsorptive isotherm curves, while the kinetic studies were carried out at different temperatures (293, 303 and 313 K), separately.

The adsorption capacity (q_e, mg g^{-1}) of unit weight of MIL-100(Fe) onto NR and removal percentage was calculated according to the following equations:

$$q_e = \frac{C_0 - C_e}{m} V \tag{1}$$

where C_0 is the initial NR concentration (mg L^{-1}), C_e is the NR concentration at any time t or equilibrium (mg L^{-1}), V is the NR solution volume (L), and m is the mass of MIL-100(Fe) (g).

2.4. Desorption and regeneration experiments

The recyclability of MIL-101(Fe) was evaluated after treatment of the used adsorbent with deionized water. Different desorbing solutions were chosen to desorb NR-loaded MIL-100(Fe) (t = 240 min, adsorbent dose = 10 mg, C_0 = 50 mg L^{-1}, T = 303 K). After desorption, the used MIL-100(Fe) was reused to adsorb NR and the adsorption condition was same with the first adsorption process. Then the best desorbing solution was chosen for the continuous desorption–adsorption studies to explore the reuse capacity of MIL-100(Fe). The desorption efficiency (D) and regeneration efficiency (η) were calculated using the following equations:

$$D = \frac{m}{m_c} \times 100\% \tag{2}$$

$$\eta = \frac{q_n}{q_e} \times 100\% \tag{3}$$

where D is the desorption efficiency of the MIL-100(Fe) (%); m is the mass of NR (g), which is desorbed from the adsorbent and m_c is the remaining NR mass on MIL-100(Fe) before desorption (g). η is regeneration efficiency of the MIL-100(Fe) (%), q_n and q_e are the adsorption quantity of regenerative MIL-100(Fe) for recycle times and the primitive MIL-100(Fe) in the same experimental conditions, respectively.

3. Results and discussion

3.1. Characterization of materials

The prepared MIL-100(Fe) was characterized by FTIR, XRD, SEM, N_2 adsorption–desorption experiment and XPS.

3.1.1. FTIR analysis

FTIR spectroscopic analysis is a vital tool to characterize both the covalent and non-covalent functional group of a substance. The FTIR spectrum of MIL-100(Fe) is shown in Fig. 3. As clearly seen from the figure, the peak at approximately 3,442 cm^{-1} represented the stretching vibration of the O–H group, whiles that at 1,638 and 1,325 cm^{-1} was due to O–H and C–O stretching vibrations, respectively [30]. Absorption peak at 548 cm^{-1} was from the stretching vibration of Fe–O bond, which clearly demonstrated that the two materials reacted successfully [31]. In addition, the result of pH_{pzc} measurement was 4.62 (figure not shown).

3.1.2. XRD and SEM analysis

The XRD pattern of the synthesized MIL-100(Fe) (b) and the simulated one (a) are shown in Fig. 4. The figure showed the characteristic peak of MIL-100(Fe) appeared nearby 10° which was in agreement with the simulated one [32], confirming the successful preparation of MIL-100(Fe). The SEM micrographs of MIL-100(Fe) are picked up in Fig. 5. It was clearly observed that the surface of MIL-100(Fe) was very rough with many apertures which aided in its ability to bind NR.

3.1.3. Surface area and pore volume analysis

N_2 adsorption–desorption isotherms based on the Barrett–Joyner–Halenda (BJH) model is obtained to further study the

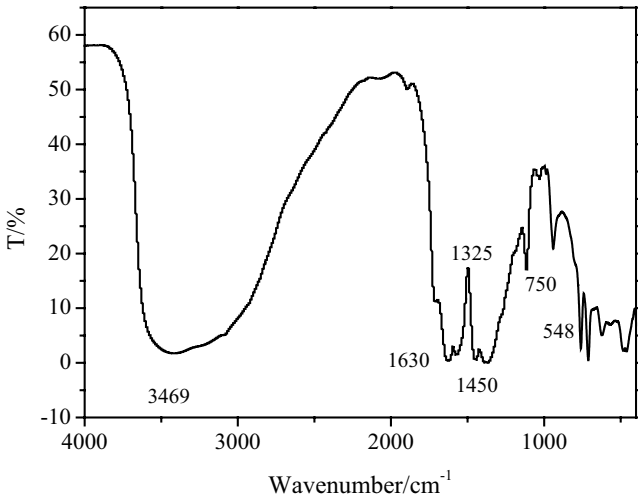

Fig. 3. FTIR spectra of MIL-100(Fe).

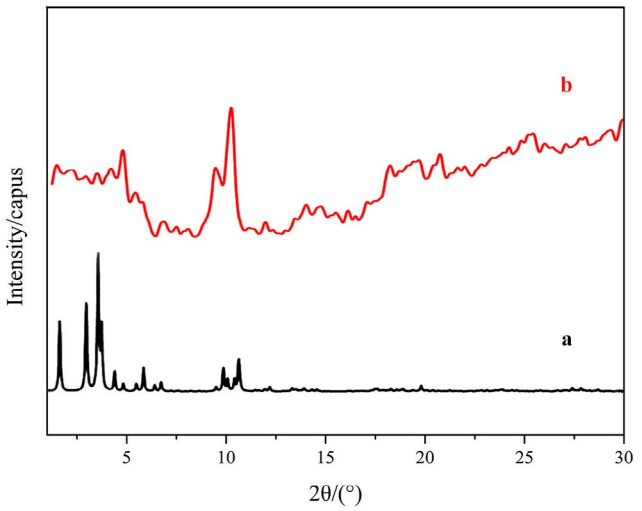

Fig. 4. XRD pattern of simulated MIL-100(Fe) (a) and MIL-100(Fe) (b).

hollow and porous structures of the products [33]. As depicted in Fig. 6, the prepared MIL-100(Fe) gave a BET surface area of 1,013 $m^2\ g^{-1}$ with a pore volume of 0.22 $cm^3\ g^{-1}$. The pore size distribution of MIL-100(Fe) estimated by using the BJH method gave an adsorption pore width in the range of 2–20 nm and the figure of aperture profile demonstrated the existence of mesopores. The relatively bigger pores can be attributed to the cavity inside the particles and granular stack.

3.1.4. XPS analysis

X-ray photoelectron spectroscopy (XPS) is used to confirm the presence of each metal as well as the different oxidation states in which they occur. XPS is very useful in calculating the ratio between the metals as well as the ratio of each oxidation state of different metals in materials [34]. The XPS spectrum in Fig. 7 indicates the presence of Fe, O, C, N elements. N element appeared after the adsorption which meant MIL-100(Fe) had adsorbed NR successfully. The core level binding energy observed for the Fe $2p_{3/2}$ primary peak at 711.83 eV was clearly different from 706.55 eV of Fe metal and 708 eV of Fe^{2+}. These peaks can be indexed to Fe^{3+} ions as they match well with reported binding energy of Fe^{3+} states. The two distinct states of Fe $2p_{1/2}$ and Fe $2p_{3/2}$ were observed at 724.39 and 711.83 eV and the peak of Fe $2p_{3/2}$ was stronger than Fe $2p_{1/2}$ due to spin–orbit splitting [35,36]. Therefore, it could be further proved that Fe was in its trivalent state. The peak of N1s at 397.6 eV belonged to Fe–N bond and the peak of O1s at 530.2 eV assigned to Fe–O bond. Meanwhile, comparing the XPS of elements from Figs. 7b and c, it is observed that the peak position of Fe2p and O1s did not change, but its relative strength decreased obviously, and the peak of N1s appeared after adsorption, which further proved the chemical adsorption taking place during the process.

The results from N_2 adsorption–desorption measurements analysis and XPS of samples before and after reaction indicated that MIL-100(Fe) had large surface area and good structural stability, which was of significance for potential applications in adsorption field.

3.2. Adsorption study

3.2.1. Effect of coexisted ions on adsorption

It is essential to study the effect of coexisted salts in solution on adsorption quantity as there are appreciable amounts of common salts in dye wastewater. The batch adsorption experiments were carried out at 50 mg L^{-1} NR solution with the initial pH of 5.35 and various concentration of five different salts. The results are shown in Fig. 8. It is noticed from Fig. 8 that similar results were obtained for five salts that the values of q_e increased as the concentration of coexisted salts increased. This may be attributed to the presence of non-electrostatic forces such as hydrogen bond and dispersive interaction. These forces were enhanced with the increase in ionic strength, which screened the electrostatic interaction. Moreover, with the development of ionic strength, the non-electrostatic forces increased, thus resulted in the relatively higher adsorption quantity. Furthermore, adsorption capacity of MOF toward NR was higher with solution containing of $CaCl_2$, $MgCl_2$ and $Zn(NO_2)_2$. The result is different from the adsorption of malachite green on MIL-100(Fe), which may be due to the different dominant roles of the two adsorption process [27].

3.2.2. Effect of pH on adsorption

Initial pH will affect the surface charge of MIL-100(Fe) and the protonation degree of NR. The solution pH has an important effect on the NR adsorption process because it determines the forms of NR in aqueous phases and the surface charge of the adsorbent, thereby affecting the adsorption process and the adsorption capacity. The results at various solution pH are presented in Fig. 9. It was obviously seen from the figure that pH had an evident effect on NR adsorption capacity. The maximum adsorption capacity of NR on MIL-100(Fe) emerged at pH 7–8. As the solution pH increased from 1 to 5, the negative charges on the surface of MIL-100(Fe) increased, which was favorable for the adsorption of positively charged NR due to electrostatic attraction. However, with the increase of pH until the pH > 8.0, the adsorption capacity of NR on

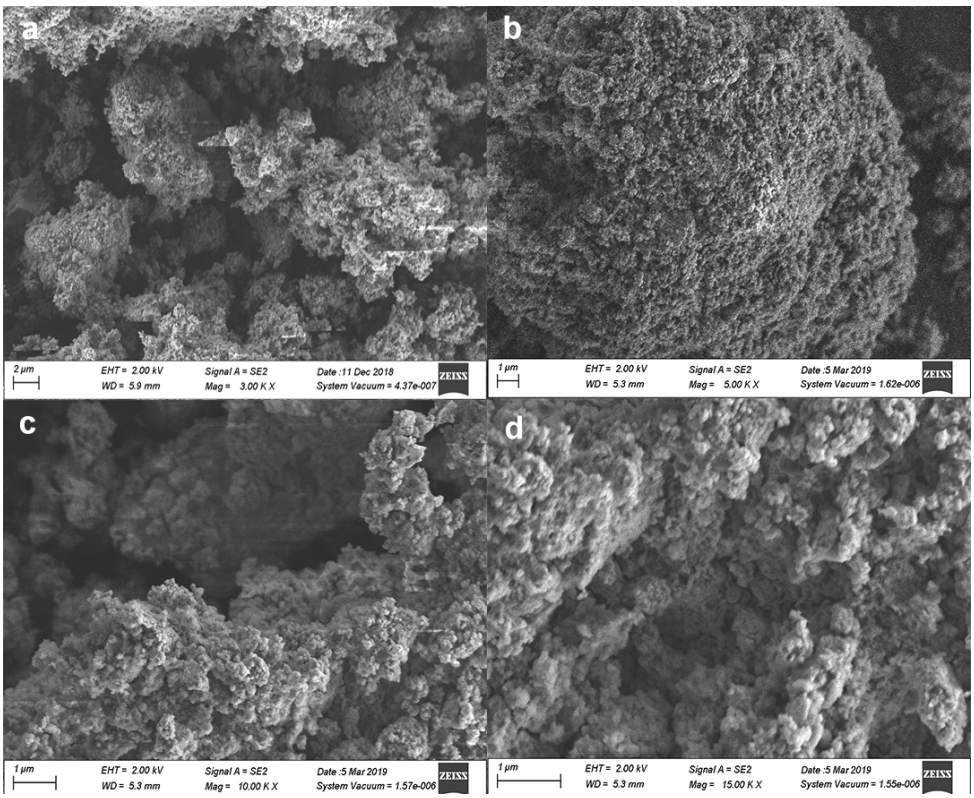

Fig. 5. SEM images of MIL-100(Fe) of different magnification.

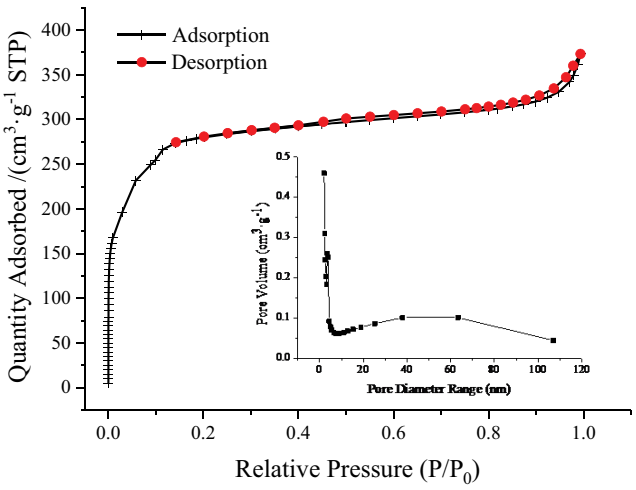

Fig. 6. N_2 adsorption–desorption and pore volume of MIL-100(Fe).

the adsorbent descended, abundance of OH^- competed with NR for adsorption, moreover, MIL-100(Fe) and the alkaline NR produced electrostatic repulsion. When the value of pH was from 7.0 to 8.0, the adsorption quantity changed little, so the initial pH was adjusted to 7–8 to achieve the best adsorption effect. But different adsorption results were observed for the methylene blue adsorption on MIL-100(Fe), which may be caused by the fact that pH is not as sensitive to methylene blue as neutral red [37].

3.2.3. Effect of equilibrium NR concentration on adsorption

The effect of equilibrium NR concentration and solution temperature on adsorption quantity was performed and the results are presented in Fig. 10. It was observed that the values of q_e had a sharp rise with the increase in NR concentration. This could be attributed to the driving force from the dye concentration gradient. The maximum values of $q_{e(\exp)}$ obtained at 293, 303 and 313 K were 320, 328 and 333 mg g^{-1}, respectively, which showed that the effect of temperature on adsorption quantity was not significant. Moreover, with the increase in temperature, the unit adsorption capacity increased, which indicated that the adsorption process was endothermic.

After adsorption equilibrium, values of C_e were less than 6.5 mg L^{-1} while the scope of initial NR concentration was from 10 to 170 mg L^{-1} (before adsorption). This showed that there was higher removal efficiency of MIL-100(Fe) toward NR from solution.

The adsorption equilibrium isotherm represents the mathematical relation of the amount of adsorbed target per gram of adsorbent to the equilibrium solution concentration at fixed temperature. It is necessary to establish the appropriate correlations for the equilibrium data in the design of the adsorption system. The adsorption isotherms are used to measure the relationship between adsorbents and adsorbates. Langmuir, Freundlich and Temkin model are used for fitting analysis of experimental data.

$$q_e = \frac{q_m K_L C_e}{1 + K_L C_e} \tag{4}$$

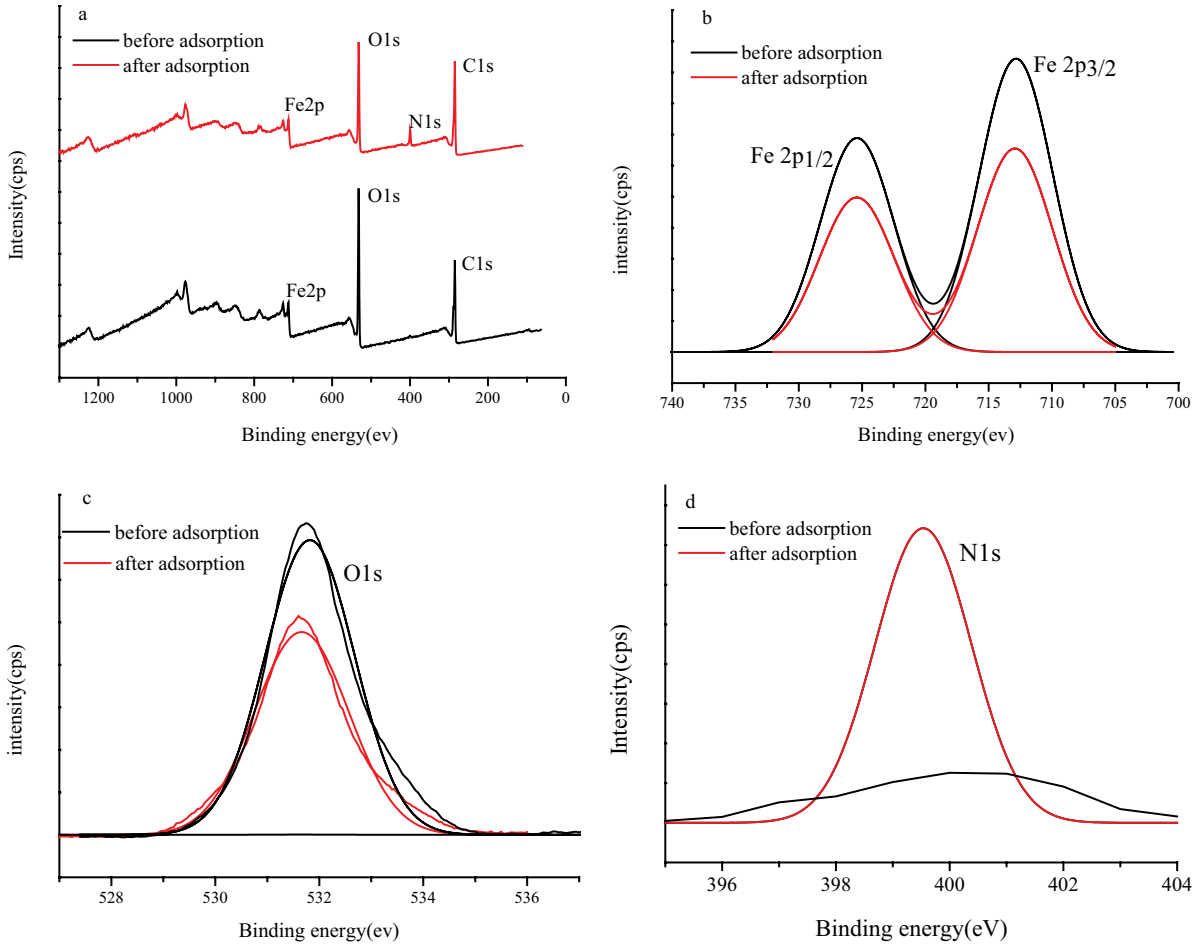

Fig. 7. Survey XPS spectrum of MIL-100(Fe) and MIL-100(Fe)/NR (a); high-resolution Fe2p, O1s and N1s XPS spectra of MIL-100(Fe) before and after adsorption of NR (b–d).

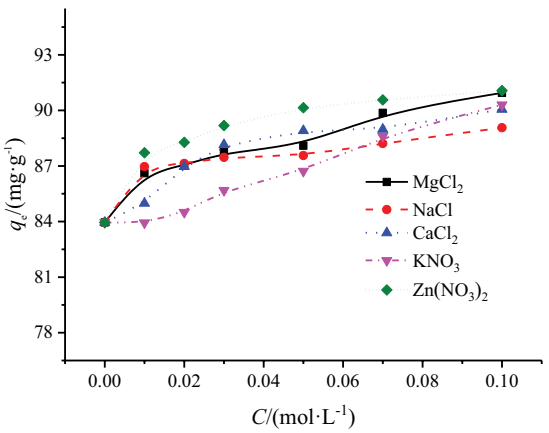

Fig. 8. Effect of salt concentration on NR adsorption.

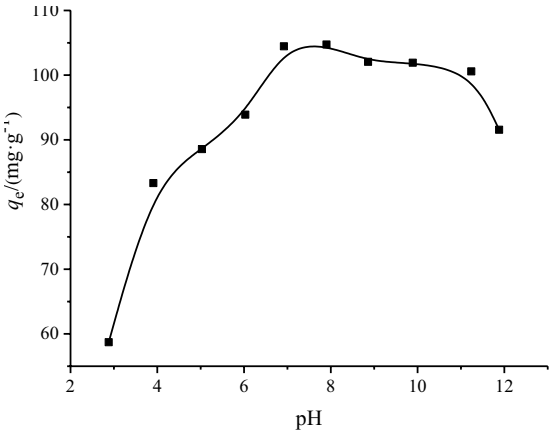

Fig. 9. Effect of solution pH on NR adsorption.

where q_e is the maximum adsorption capacity (mg g^{-1}), q_m is the equilibrium adsorption capacity (mg g^{-1}), K_L is a constant related to the affinity of the binding sites and energy of adsorption (L mg^{-1}). C_e is equilibrium concentration (mg L^{-1}).

$$q_e = K_F C_e^{1/n} \quad (5)$$

where K_F is the constant of the Freundlich isotherm, $1/n$ is the constant which is related to the adsorption capacity and the adsorption intensity.

$$q_e = A + B\ln C_e \quad (6)$$

where A and B are the Temkin isotherm constants.

Nonlinear regressive analysis is used to fit the data using adsorption models and the fitted results are listed in Table 1. The fitted curves are also presented in Fig. 10.

It was observed that values of R^2 obtained from Temkin equation were higher while the values of SSE were lower than other two equilibrium models. Furthermore, the fitted curves from Temkin equation were more close to the experimental curves. This shows that the Temkin equation was better to describe the adsorption process than Langmuir model and Freundlich model which was heterogeneous adsorption on multilayer surface. According to the fitted results, Langmuir model was also used to describe the equilibrium process while Freundlich model was the least to predict the process. The comparison of NR adsorption capacity on MIL-100(Fe) and other adsorbents is listed in Table 2. Obviously, MIL-100(Fe) had a larger adsorption capacity than traditional adsorbent, which indicated that it had some prospects for practical application.

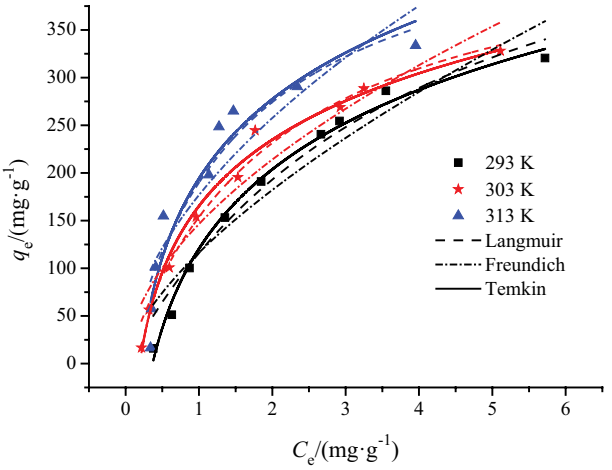

Fig. 10. Adsorption isotherms and fitted curves.

3.2.4. Adsorption kinetic study

The kinetic study was carried out at different initial NR concentration and temperature, the kinetics data (shown in Fig. 11) obtained from batch adsorption studies indicated that q_t had a sharp increase within the first 1 h and then reached a plateau with different concentration, respectively.

In order to explore the adsorption mechanism of MIL-100(Fe) on NR and figure out what controls the process, kinetic analysis were performed, the pseudo-first-order kinetic model and pseudo-second-order kinetic model were used for fitting analysis of experimental data.

$$q_t = q_e(1 - e^{-k_1 t}) \tag{7}$$

$$q_t = \frac{k_2 q_e^2 t}{1 + k_2 q_e t} \tag{8}$$

where q_t is adsorption quantity (mg g^{-1}) at time t, q_e is adsorption quantity at equilibrium (mg g^{-1}); k_1 (min^{-1}) and k_2 (mg g^{-1} min^{-1}) are kinetic rate constants of pseudo-first-order kinetic model and pseudo-second-order kinetic model, respectively.

Table 2
Comparison of adsorption capacity of NR onto various adsorbents

Adsorbent	q_e (mg g^{-1})	Reference
Pyrolytic char	62.3	[38]
Activated carbon fiber	20.7	[39]
Mesoporous carbon spheres	227.3	[40]
Peanut husk	37.5	[41]
TOC-$MnCl_2$	198.3	[42]
$Zn_3[Co(CN)_6]_2{\cdot}nH_2O$ nanospheres	285.7	[43]
MIL-100(Fe)	333.3	This study

Table 1
Parameters of equilibrium models

Langmuir					
T/K	K_L (L mg^{-1})	$q_{e\,(exp)}$/(mg g^{-1})	$q_{m\,(theo)}$/(mg g^{-1})	R^2	SSE × 10^3
293	0.252 ± 0.067	320	455 ± 86	0.964	2.821
303	0.489 ± 0.087	328	467 ± 38	0.978	1.753
313	0.624 ± 0.230	333	493 ± 88	0.891	9.187
Freundlich					
T/K	K_F	$1/n$	R^2	SSE × 10^4	
293	116 ± 13	0.646 ± 0.087	0.914	6.772	
303	146 ± 12	0.547 ± 0.069	0.928	5.960	
313	176 ± 17	0.542 ± 0.103	0.813	1.573	
Temkin					
T/K	A	B	R^2	SSE × 10^3	
293	120 ± 3.4	120 ± 3.6	0.991	0.681	
303	165 ± 3.7	100 ± 3.3	0.988	0.963	
313	194 ± 10	120 ± 12	0.924	6.322	

Note: SSE = $\sum(q - q_c)^2$, q and q_c are the experimental value and calculated value according to the model, respectively.

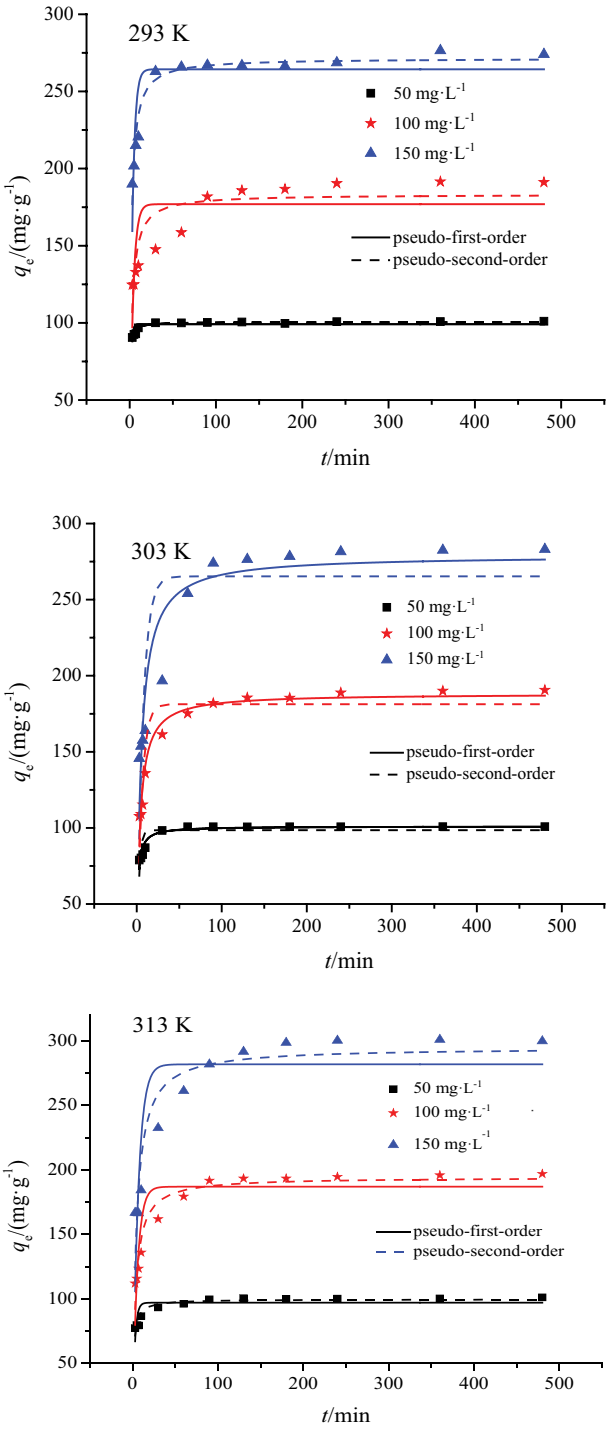

Fig. 11. Adsorption kinetic process and fitted curves.

Values of k, q_e, and R^2 are listed in Table 3 using nonlinear regressive analysis and the fitted curves are also shown in Fig. 11. It was seen that the equilibrium adsorption capacity increased from 100.8 to 283.1 mg g^{-1} with the increase in initial NR concentration from 50 to 150 mg L^{-1} at 293 K, and the calculated q_e values had good agreement with the experimental values. Furthermore, there were higher values of R^2 and lower values of SSE from this model. So NR adsorption on MIL-100(Fe) followed the pseudo-second-order kinetic model, which indicated that there was chemical adsorption between MIL-100(Fe) and NR.

3.2.5. Thermodynamic parameters

Thermodynamic parameters including enthalpy change (ΔH^o), Gibbs free energy change (ΔG^o) and entropy change (ΔS^o) were used to estimate the effect of temperature on the adsorption of NR on MIL-100(Fe). They can be determined using the following equations.

$$K_c = \frac{C_{ad,e}}{C_e} \tag{9}$$

$$\Delta G° = -RT \ln K_c \tag{10}$$

$$\Delta G° = \Delta H° - T\Delta S° \tag{11}$$

where K_c is the distribution coefficient for the adsorption, $C_{ad,e}$ is the concentration of NR on the adsorbent at equilibrium (mg L^{-1}), R (8.314 J mol^{-1} K^{-1}) is the universal gas constant, T is the temperature (K).

The activation energy (E_a) is a physical quantity related to the rate of reaction, and its value can be used to infer the speed of the adsorption process. The activation energy for NR adsorption was calculated by the Arrhenius equation, the linear form is given as follows:

$$\ln k_2 = \ln k_0 - \frac{E_a}{RT} \tag{14}$$

where k_0 (g mg^{-1} min^{-1}) is the temperature independent factor, E_a (kJ mol^{-1}) is the apparent activation energy of the reaction of adsorption, R is the gas constant, 8.314 J mol^{-1} K^{-1} and T (K) is the adsorption absolute temperature. When $\ln k_2$ is plotted vs. $1/T$, a straight line with slope $-E_a/R$ is obtained.

The thermodynamic parameters are listed in Table 4. The negative values of $\Delta G°$ at various temperatures were due to the fact that the adsorption process was spontaneous. The positive value of $\Delta H°$ showed that the reaction was endothermic, and also showed that higher temperature was beneficial to the reaction. The negative $\Delta S°$ for NR on MIL-100(Fe) showed that this was one process of entropy decrease. The value of E_a < 40 kJ mol^{-1} was due to the result of physical adsorption process. The value of E_a was 27.5 kJ mol^{-1}, confirming the occurrence of physical action in the adsorption process.

3.2.6. Regeneration and reuse

Reuse of exhausted adsorbent or recovery of the adsorbate loaded on the adsorbent will make the treatment process economical thus it is necessary to generate the exhausted adsorbent after adsorption [44–47]. In order to study the recycling performance of materials, the cyclic adsorption of MIL-100(Fe) by different materials is preliminarily tested, and three materials are used for further cyclic research. The results are presented in Fig. 12. It is obviously found from Fig. 12 that the adsorption capacity of NR on MIL-100(Fe) decreased with the increase in recycle number. HCl solution was the least results of regeneration. After three cycles of

Table 3
Parameters of kinetic models for NR adsorption onto MIL-100(Fe)

Pseudo–first–order equation						
T/K	C_0 (mg L^{-1})	$q_{e\,(exp)}$/(mg g^{-1})	$q_{e\,(theo)}$/(mg g^{-1})	k_1	R^2	SSE × 10^3
293	50	101	99 ± 0.8	0.392 ± 0.057	0.551	0.391
	100	191	176 ± 6.1	0.185 ± 0.026	0.777	2.633
	150	274	264 ± 5.5	0.157 ± 0.028	0.714	9.882
303	50	100	98 ± 1.2	0.397 ± 0.054	0.582	0.351
	100	190	181 ± 5.7	0.181 ± 0.024	0.813	2.130
	150	283	265 ± 11.0	0.144 ± 0.028	0.709	10.201
313	50	101	97 ± 2.4	0.732 ± 0.083	0.493	0.073
	100	196	186 ± 5.3	0.265 ± 0.051	0.548	3.332
	150	299	281 ± 11.3	0.308 ± 0.037	0.736	2.607
Pseudo-second-order equation						
T/K	C_0 (mg L^{-1})	$q_{e\,(exp)}$/(mg g^{-1})	$q_{e\,(theo)}$/(mg g^{-1})	k_2 × 10^{-3}	R^2	SSE × 10^3
293	50	101	100 ± 0.3	8.501 ± 1.122	0.893	0.092
	100	191	183 ± 4.1	1.554 ± 0.213	0.931	0.820
	150	274	271 ± 2.5	0.812 ± 0.157	0.881	0.417
303	50	100	101 ± 1.0	8.731 ± 1.022	0.912	0.072
	100	190	188 ± 3.9	1.570 ± 0.183	0.943	0.645
	150	283	279 ± 8.4	0.755 ± 0.153	0.871	4.552
313	50	101	99 ± 1.8	0.022 ± 0.034	0.928	0.013
	100	196	194 ± 3.2	2.559 ± 0.563	0.885	1.584
	150	299	294 ± 8.2	2.301 ± 0.227	0.950	0.457

Table 4
Thermodynamic parameters of adsorption

E_a	$\Delta H°$	$\Delta S°$	$\Delta G°$ (kJ mol^{-1})		
(kJ mol^{-1})	(kJ mol^{-1})	(kJ mol^{-1} K^{-1})	293 K	303 K	313 K
27.50	29.52	–0.14	–11.50	–12.91	–14.33

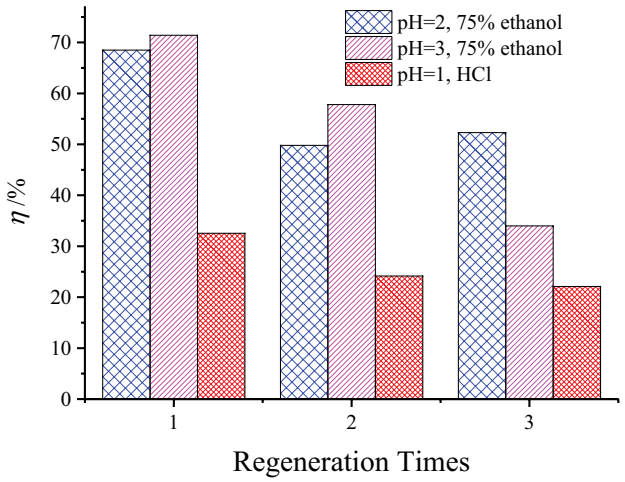

Fig. 12. Regeneration rate of three cycles using various solutions.

adsorption, the adsorption amount by 75% ethanol with pH 2 and 3 decreased by 16.3% and 27.4%, respectively. This may be because the chemical desorption process is not complete, resulting in partial dye molecules still remaining in the pore structure of MIL-100(Fe), reducing the specific surface area of MIL-100(Fe) during the cyclic adsorption process, thus reducing the adsorption of dyes. The first desorption and regeneration rate of MIL-100(Fe) can reach 70%, the adsorption rate of NR was still 50% after three regeneration and reuse cycles by 75% ethanol with pH 2, indicating that MIL-100(Fe) after adsorption had high stability as before. The effect of contact time on desorption is carried out and results are shown in Fig. 13. It is clearly seen from Fig. 13 that the desorption efficiency reached the balance at first 100 min, then reached equilibrium. Two kinetic models were applied to fit the data and the fitting results (also shown in Fig. 13) showed that the pseudo-second-order kinetic model was better to describe the process because of the parameters of higher R^2 and lower SSE, which indicated that chemical desorption was the leading role. Similar results were observed about desorption study of 2,4-dichlorophenol-loaded surfactant-modified phoenix tree leaf and *p*-chlorophenol or *p*-nitrophenol-loaded magnetic activated carbon using NaOH solution as elution agent [48,49].

In general, MIL-100(Fe) can be used as an adsorbent for regeneration and reuse.

3.2.7. Adsorption mechanism

The results of isotherm fitting showed that the adsorption process was multilayer taking place on a heterogeneous surface. The results of kinetic and thermodynamic analysis showed that the chemical and physical adsorption of NR on MIL-100(Fe) occurred simultaneously. Due to the influence

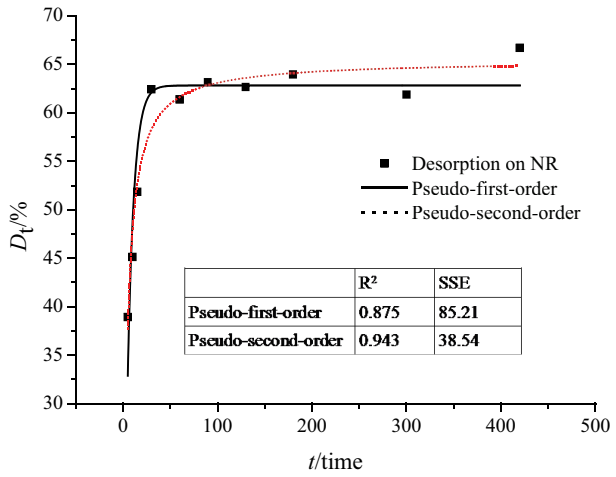

Fig. 13. Desorption kinetic process and fitted curves using 75% ethanol (pH = 2).

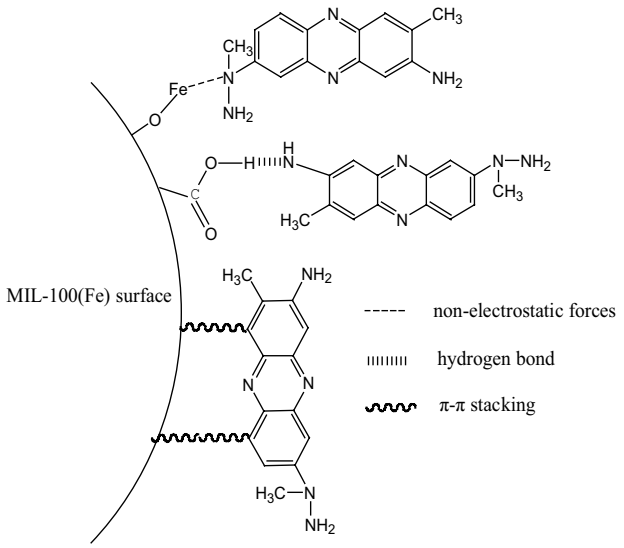

Fig. 14. Plausible mechanism for the adsorption of NR over MIL-100(Fe).

of pH and coexisting ions on the adsorption quantity, it can be concluded that ion exchange was not dominant, but rather electrostatic attraction and π–π stacking were the main adsorption mechanisms, which alludes to physical adsorption being the main mode for adsorption. The mechanism diagram is shown in Fig. 14.

3.3. Process design for single-stage batch adsorber

Adsorption isotherms can be used to predict the equilibrium results from isotherm curves and employed in the design of single adsorptive system in batch mode [50].

The design objective was to reduce initial NR concentration from C_0 to C_t with some solution volume (L).

The mass balance for NR in the single-stage operation under equilibrium is given by:

$$V(C_0-C_e)=m\cdot q_e \quad (15)$$

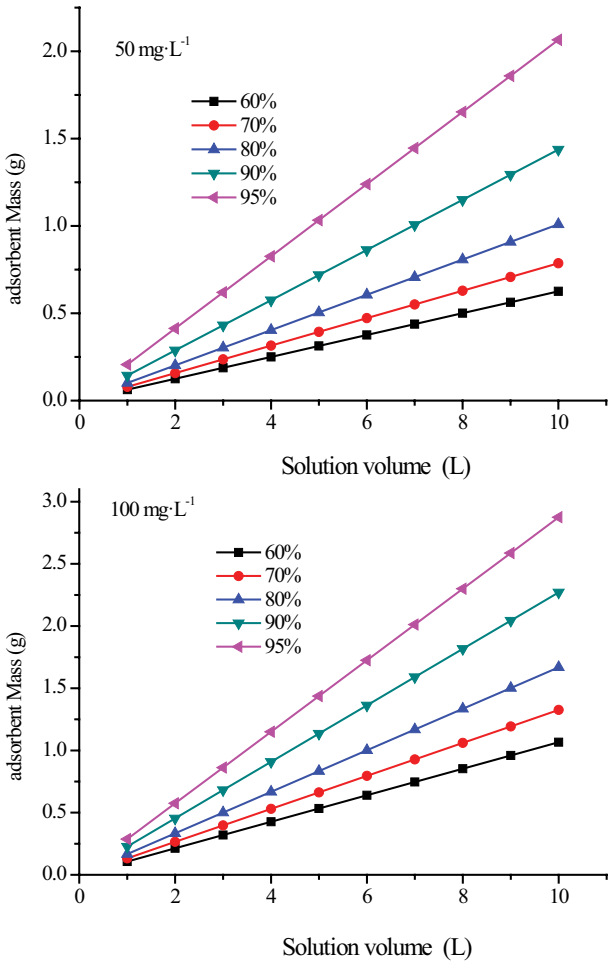

Fig. 15. Adsorbent mass (g) against solution volume (L) at various NR concentrations.

where m is amount of added adsorbent (g) and L is solution volume (L).

As Temkin model is best to describe the equilibrium data from isotherm study, this model is applied to design single-stage adsorption system. Concatenating Eq. (15) and Temkin curve through two expressions of q_e, the equation can be arranged as:

$$\frac{m}{V}=\frac{C_0-C_e}{q_e}=\frac{C_0-C_e}{A+B\ln C_e} \quad (16)$$

Fig. 15 represents several plots derived from Eq. (16). These plots showed the predicted adsorbent mass required to remove NR (C_0 = 50 and 100 mg L^{-1}) for 60%, 70%, 80%, 90% and 95% removal efficiency at various solution volume for a single-stage batch adsorption system (303 K). Usually, there was higher mass with the increase of removal efficiency at same volume or higher NR concentration.

4. Conclusion

A method for the synthesis of MIL-100(Fe) for the effective removal of NR has been presented. Characterization of the adsorbent using the FTIR spectroscopy revealed the

corresponding to the functional groups of the MIL-100(Fe) framework. As part of investigating the nature of the interface formed between the host and the guest species, an XPS analysis had been conducted which confirmed the existence of C–O–Fe bonding between the H_3BTC and MIL-100(Fe) thus confirming the results from the FTIR study. The BET surface area was 1,013 $m^2 g^{-1}$. Studies on the kinetic process indicated that the rates of dye adsorption onto MIL-100(Fe) followed the pseudo-second-order kinetic model, indicating the possibility of chemical adsorption between NR and the surfaces of MIL-100(Fe). The equilibrium adsorption isotherm was in agreement with the Temkin model. The removal efficiency of dyes increased in weakly alkaline solution, and the addition of salt had a slight positive influence on the adsorption capacity. There was some property of regeneration and reuse for NR-loaded MIL-100(Fe). The thermodynamic analysis showed that the system was spontaneous, endothermic and physical process in nature.

References

[1] K. Smith, S. Liu, Y. Liu, S. Guo, Can China reduce energy for water? A review of energy for urban water supply and wastewater treatment and suggestions for change, Renew. Sust. Energy Rev., 91 (2018) 41–58.

[2] K.G. Pavithra, S.K. P, J. V, S.R. P, Removal of colorants from wastewater: a review on sources and treatment strategies, J. Ind. Eng. Chem., 75 (2019) 1–19.

[3] M.T. Yagub, T.K. Sen, S. Afroze, H.M. Ang, Dye and its removal from aqueous solution by adsorption: a review, Adv. Colloid Interface Sci., 209 (2014) 172–184.

[4] Y. Zhou, J. Lu, Y. Zhou, Y. Liu, Recent advances for dyes removal using novel adsorbents: a review, Environ. Pollut., 252 (2019) 352–365.

[5] Y.Y. Hu, R.P. Han, Selective and efficient removal of anionic dyes from solution by zirconium (IV) hydroxide coated magnetic materials, J. Chem. Eng. Data, 64 (2019) 791–799.

[6] X. Xu, B.Y. Gao, B. Jin, Q.Y. Yue, Removal of anionic pollutants from liquids by biomass materials: a review, J. Mol. Liq., 215 (2016) 565–595.

[7] J.Y. Song, W.H. Zou, Y.Y. Bian, F.Y. Su, R.P. Han, Adsorption characteristics of methylene blue by peanut husk in batch and column modes, Desalination, 265 (2011) 119–125.

[8] T. Zhou, W.Z. Lu, L.F. Liu, H.M. Zhu, Y.B. Jiao, S.S. Zhang, R.P. Han, Effective adsorption of light green anionic dye from solution by CPB modified peanut in column mode, J. Mol. Liq., 211 (2015) 909–914.

[9] C.Y. Teh, P.M. Budiman, K.P.Y. Shak, T.Y. Wu, Recent advancement of coagulation–flocculation and its application in wastewater treatment, Ind. Eng. Chem. Res., 55 (2016) 4363–4389.

[10] J.N. Hakizimana, B. Gourich, M. Chafi, Y. Stiriba, C. Vial, P. Drogui, J. Naja, Electrocoagulation process in water treatment: A review of electrocoagulation modeling approaches, Desalination, 404 (2017) 1–21.

[11] M. Bilal, M. Adeel, T. Rasheed, Y. Zhao, H.M.N. Iqbal, Emerging contaminants of high concern and their enzyme-assisted biodegradation - a review, Environ. Int., 124 (2019) 336–353.

[12] D. Ayodhya, G. Veerabhadram, A review on recent advances in photodegradation of dyes using doped and heterojunction based semiconductor metal sulfide nanostructures for environmental protection, Mater. Today Energy, 9 (2018) 83–113.

[13] D. Kanakaraju, B.D. Glass, M. Oelgemöller, Advanced oxidation process-mediated removal of pharmaceuticals from water: a review, J. Environ. Manage., 219 (2018) 189–207.

[14] D.B. Miklos, C. Remy, M. Jekel, K.G. Linden, J.E. Drewes, U. Hübner, Evaluation of advanced oxidation processes for water and wastewater treatment-a critical review, Water Res., 139 (2018) 118–131.

[15] S.D. Gisi, G. Lofrano, M. Grassi, M. Notarnicola, Characteristics and adsorption capacities of low-cost sorbents for wastewater treatment: a review, Sustain. Mater. Technol., 9 (2016) 10–40.

[16] S. Dhaka, R. Kumar, A. Deep, M.B. Kurade, S.W. Ji, B.H. Jeon, Metal–organic frameworks (MOFs) for the removal of emerging contaminants from aquatic environments, Coordin. Chem. Rev., 380 (2019) 330–352.

[17] P. Serra-Crespo, E.V. Ramos-Fernandez, J. Gascon, F. Kapteijn, Synthesis and characterization of an amino functionalized MIL-101(Al): separation and catalytic properties. Chem. Mater., 23 (2011) 2565–2572.

[18] Y.N. Wu, F.T. Li, Y.X. Xu, W. Zhu, C.A. Tao, J.C. Cui, G.T. Li, Facile fabrication of photonic MOF films through stepwise deposition on a colloid crystal substrate. Chem. Commun., 47 (2011) 10094–10096.

[19] W.B. Lin, Homochiral porous metal-organic frameworks: why and how?, J. Solid State Chem., 178 (2005) 2486–2490.

[20] R.G. El-sharkawy, A.S. El-din, H.E.S. El-din, Kinetics and mechanism of the heterogeneous catalyzedoxidative decolorization of Acid-Blue 92 using bimetallic metal-organic frameworks, Spectrochim. Acta A, 79 (2011) 1969–1975.

[21] F.M. Mulder, T.J. Dingemans, H.G. Schimmel, A.J. Ramirez-Cuesta, G.J. Kearley, Hydrogen adsorption strength and sites in the metal organic framework MOF5: comparing experiment and model calculations, Chem. Phys., 351 (2008) 72–76.

[22] P. Song, Y.Q. Li, B. He, J.Z. Yang, J. Zheng, X.G. Li, Hydrogen storage properties of two pillared-layer Ni(II) metal-organic frameworks, Microporous Mesoporous Mater., 142 (2011) 208–213.

[23] D.T. de Lill, A. de Bettencourt-Dias, C.L. Cahill, Exploring lanthanide luminescence in Metal-Organic Frameworks: synthesis, structure, and guest-sensitized luminescence of a mixed Europium/Terbium-Adipate Framework and a Terbium-Adipate Framework, Inorg. Chem., 46 (2007) 3960–3965.

[24] B.L. Chen, L.B. Wang, F. Zapata, G.D. Qian, E.B. Lobkovsky, A luminescent microporous metal-organic framework for the recognition and sensing of anions, J. Am. Chem. Soc., 130 (2008) 6718–6719.

[25] Q.X. Jia, Y.Q. Wang, Q. Yue, Q.L. Wang, E.Q. Gao, Isomorphous Co-II and Mn-II materials of tetrazolate-5-carboxylate with an unprecedented self-penetrating net and distinct magnetic behaviors, Chem. Commun., 40 (2008) 4894–4896.

[26] E. Haque, J.W. Jun, S.H. Jhung, Adsorptive removal of methyl orange and methylene blue from aqueous solution with a metal-organic framework material, iron terephthalate (MOF-235), J. Hazard. Mater., 185 (2011) 507–511.

[27] T. Rajkumar, D. Kukkar, K.-H. Kim, J.R. Sohn, A. Deep, Cyclodextrin-metal–organic framework (CD-MOF): from synthesis to applications, J. Ind. Eng. Chem., 72 (2019) 50–66.

[28] S.H. Huo, X.P. Yan, Metal–organic framework MIL-100(Fe) for the adsorption of malachite green from aqueous solution, J. Mater. Chem., 22 (2012) 7449–7455.

[29] P. Horcajada, S.C. SurbléS, Synthesis and catalytic properties of MIL-100 (Fe), an iron (iii) carboxylate with large pores, Chem. Commun., 27 (2007) 2820–2822.

[30] E. Murugan, S. Arumugam, New dendrimer functionalized multi-walled carbon nanotube hybrids for bone tissue engineering, RSC Adv., 4 (2014) 35428–35441.

[31] J.X. Xie, W.J. Chen, Y.Y. Wu, X.X. Wu, Highly efficient adsorption capacity of MIL-53(Fe) metal organic framework material for Congo red, Ind. Water Treat., 37 (2017) 27–30.

[32] F. Zhang, M.Y. Zhang, K.Q. Zhang, Preparation and characterization of MIL-100(Fe) and its catalytic performance in knoevenagel condensation, New. Chem. Mater., 45 (2017) 69–72.

[33] S.R. Ali, V.K. Bansal, A.A. Khan, S.K. Jain, M.A. Ansari, Growth of zinc hexacyanoferrate nanocubes and their potential as heterogeneous catalyst for solvent-free oxidation of benzyl alcohol, J. Mol. Catal., A, 303 (2009) 60–64.

[34] N.A. Sitnikova, M.A. Komkova, I.V. Khomyakova, E.E. Karyakina, A.A. Karyakin, Transition metal hexacyanoferrates in electrocatalysis of H_2O_2 reduction: an exclusive property of Prussian Blue, Anal. Chem., 86 (2014) 4131–4134.

[35] T. Yamashita, P. Hayes, Analysis of XPS spectra of Fe^{2+} and Fe^{3+} ions in oxide materials, Appl. Surf. Sci., 254 (2008) 2441–2449.
[36] Y. Jia, Q. Jin, Y. Li, Y. Sun, J. Huo, X. Zhao, Investigation of the adsorption behaviour of different types of dyes on MIL-100(Fe) and their removal from natural water, Anal. Method., 7 (2015) 1463–1470.
[37] S.J. Gerber, E. Erasmus, Electronic effects of metal hexacyanoferrates: An XPS and FTIR study, Mater. Chem. Phys., 203 (2018) 73–81.
[38] W.H. Zou, H.J. Bai, S.P. Gao, Competitive adsorption of neutral red and Cu^{2+} onto Pyrolytic Char: isotherm and kinetic study, J. Chem. Eng. Data., 57 (2012) 2792–2801.
[39] L. Zhang, L.Y. Tu, Y. Liang, Q. Chen, Z.S. Li, C.H. Li, Z.H. Wang, W. Li, Coconut-based activated carbon fibers for efficient adsorption of various organic dyes, RSC. Adv., 8 (2018) 42280–42291.
[40] Y. Tian, S.N. Zhong, X.J. Zhu, A.L. Huang, Y.Z. Chen, X.F. Wang, Mesoporous carbon spheres: synthesis, surface modification and neutral red adsorption, Mater. Lett., 161 (2015) 656–660.
[41] R.P. Han, P. Han, Z.H. Cai, Z.H. Zhao, M.S. Tang, Kinetics and isotherms of Neutral Red adsorption on peanut husk, J. Environ. Sci., 20 (2008) 1035–1041.
[42] J. Zhang, Q.Q. Shi, C.L. Zhang, J.T. Xu, B. Zhai, B. Zhang, Adsorption of Neutral Red onto Mn-impregnated activated carbons prepared from *Typha orientalis*, Bioresour. Technol., 99 (2008) 8974–8980.
[43] W.Q. Wang, C.C. Li, J.L. Yao, B. Zhang, Y.T. Zhang, J.D. Liu, Rapid adsorption of neutral red from aqueous solutions by $Zn_3[Co(CN)_6]_2{\cdot}nH_2O$ nanospheres, J. Mol. Liq., 184 (2013) 10–16.
[44] R.D. Zhang, J.H. Zhang, X.N. Zhang, C.C. Dou, R.P. Han, Adsorption of Congo red from aqueous solutions using cationic surfactant modified wheat straw in batch mode: kinetic and equilibrium study, J. Taiwan Inst. Chem. Eng., 45 (2014) 2578–2583.
[45] B.L. Zhao, W. Xiao, Y. Shang, H.M. Zhu, R.P. Han, Adsorption of light green anionic dye using cationic surfactant-modified peanut husk in batch mode, Arab. J. Chem., 10 (2017) S3595–S3602.
[46] Y.N. Shang, X. Xu, B.Y. Gao, Q.Y. Yue, Highly selective and efficient removal of fluoride from aqueous solution by Zr-La dual-metal hydroxide anchored bio-sorbents, J. Clean. Prod., 199 (2018) 36–46.
[47] Y.F. Gu, M.Y. Liu, M.M. Yang, W.L. Wang, S.S. Zhang, R.P. Han, Adsorption of light green anionic dye from solution using polyethyleneimine-modified carbon nanotubes in batch mode, Desal. Wat. Treat., 138 (2019) 368–378.
[48] X.F. Ren, R.D. Zhang, W.Z. Lu, T. Zhou, R.P. Han, S.S. Zhang, Adsorption potential of 2,4-dichlorophenol onto cationic surfactant-modified Phoenix tree leaf in batch mode, Desal. Wat. Treat., 57 (2016) 6333–6346.
[49] Y.C. Rong, R.P. Han, Adsorption of p-chlorophenol and p-nitrophenol in single and binary systems from solution using magnetic activated carbon, Korean J. Chem. Eng., 36 (2019) 942–953.
[50] S. Dawood, T.K. Sen, Removal of anionic dye Congo red from aqueous solution by raw pine and acid-treated pine cone powder as adsorbent: equilibrium, thermodynamic, kinetics, mechanism and process design, Water Res., 46 (2012) 1933–1946.